ELSEVIER

Diamond and Related Materials 9 (2000) 771–776

DIAMOND AND RELATED MATERIALS

www.elsevier.com/locate/diamond

Density, sp^3 content and internal layering of DLC films by X-ray reflectivity and electron energy loss spectroscopy

A. LiBassi [a], A.C. Ferrari [b,*], V. Stolojan [c], B.K. Tanner [a], J. Robertson [b], L.M. Brown [c]

[a] *Department of Physics, University of Durham, Durham DH1 3LE, UK*
[b] *Department of Engineering, University of Cambridge, Cambridge CB2 1PZ, UK*
[c] *Cavendish Laboratories, University of Cambridge, Cambridge CB3 OHE, UK*

Abstract

A variety of hydrogenated and non-hydrogenated amorphous carbon thin films have been characterised by means of grazing-incidence X-ray reflectivity (XRR) to give information about their density, thickness, surface roughness and layering. We used XRR to validate the density of ta-C, ta-C:H and a-C:H films derived from the valence plasmon in electron energy loss spectroscopy measurements, up to 3.26 and 2.39 g/cm^3 for ta-C and ta-C:H, respectively. By comparing XRR and electron energy loss spectroscopy (EELS) data, we have been able for the first time to fit a common electron effective mass of $m^*/m_e = 0.87$ for all amorphous carbons and diamond, validating the 'quasi-free' electron approach to density from valence plasmon energy. While hydrogenated films are found to be substantially uniform in density across the film, ta-C films grown by the filtered cathodic vacuum arc (FCVA) show a multilayer structure. However, ta-C films grown with an S-bend filter show a high uniformity and only a slight dependence on the substrate bias of both sp^3 and layering. © 2000 Elsevier Science S.A. All rights reserved.

Keywords: Diamond-like carbon; Electron spectroscopy; X-ray reflectivity

1. Introduction

Density, sp^3 fraction, clustering of the sp^2 phase, hydrogen content and internal layering are the key structural parameters that determine the properties of amorphous carbons. Electron energy loss spectroscopy (EELS) is presently the method of choice for sp^3 measurements, from the size of the π^* peak in the carbon K edge absorption spectrum, and the mass density can be deduced from the valence plasmon energy. Here, we show how grazing incidence X-ray reflectivity (XRR) can be used to obtain information about density, roughness and cross-sectional layering for any amorphous carbon, without any sample preparation or damage [1–5]. This is a great advantage over EELS. Furthermore, XRR can give information about the possible layering within the films. This could be obtained by cross-sectional EELS, but only with complex and careful sample preparation [6].

XRR gives information about the total electron density, which can be directly translated into mass density [5]. However, density determinations via EELS rely on an effective electron mass, for which different values can be found in literature [7–9], but so far, no attempt to directly measure it for amorphous carbons has been outlined. Comparison with Rutherford backscattering (RBS) or flotation measurements has been the main way to benchmark EELS density [7–9], but these independent density determinations sometimes disagreed with EELS [8,9]. We will show how a correct fit of the plasmon peak and an appropriate choice of the effective mass can give a good agreement with the XRR mean densities, thus validating the use of the 'quasi-free' electron model to analyse the low loss spectrum. Indeed, a unique effective mass for all amorphous carbons and diamond is obtained for the first time.

2. Experimental

2.1. Samples

The samples analysed in this paper are tetrahedral amorphous carbon, ta-C, hydrogenated ta-C, ta-C:H,

* Corresponding author. Fax: +44-1223-332662.
E-mail address: acf26@eng.cam.ac.uk (A.C. Ferrari)

0925-9635/00/$ - see front matter © 2000 Elsevier Science S.A. All rights reserved.
PII: S0925-9635(99)00233-2

amorphous carbon (hydrogenated) a-C: (H), and nanostructured a-C, all deposited on Si. Two sets of ta-C films were analysed. The first, deposited using a single bend filtered cathodic vacuum arc (FCVA) system [8] with a different bias: −290, −200, −80 V, floating potential, +10 V. The second series of ta-C films was deposited at −20, −100 and −300 V on an S-Bend FCVA [10]. Two series of ta-C:H samples were obtained using two electron cyclotron wave resonance sources (one slightly capacitively coupled) with an acetylene plasma and an ion energy ranging from 80 to 170 eV [11]. A value of approximately 30 at.% H for all the films was derived by elastic recoil detection analysis (ERDA) [11]. One ta-C:H was deposited from methane with a plasma beam source [12], and ERDA analysis gave a value of ∼40 at.% H. Two a-C:H were deposited from methane using a PECVD reactor with an estimated H content of ∼40 at.%. An a-C sample was deposited by d.c. magnetron sputtering, and a nanostructured a-C film was produced by deposition of supersonic carbon cluster beams generated by a pulsed plasma cluster source [13].

2.2. XRR and EELS

Specular reflectivity curves were acquired with a Bede Scientific GIXR reflectometer, equipped with a Bede EDRa scintillation detector, using CuK_β radiation (λ= 1.3926 Å). Specular and off-specular reflectivity curves were measured for each sample, with the incidence angle θ_i usually varying in the range 0–8000 arcseconds, with a step of 20 arcseconds.

By fitting the XRR data to simulated curves, the material parameters can be obtained. Simulations were performed using the Bede REFS-MERCURY software package, which uses Parrat's recursive formalism of the Fresnel equations to calculate the reflected wave amplitude and, hence, the reflected intensity [5,14–16]. XRR probes the atomic-scale surface roughness, which results in X-rays being scattered out of the specular beam, causing a reduction in the specular reflected intensity. The intensity fall is faster than $(2\theta)^{-4}$, which holds for a perfectly smooth surface. By combining specular and diffuse scatter, genuine surface roughness can be separated from compositional grading [15]. Surface and interface roughness was incorporated within the distorted Born wave approximation using a Gaussian variation of the electron density gradient, so that the values given below are r.m.s. roughnesses. XRR probes a macroscopic area of the sample (∼cm^2). This is particularly significant for roughness measurements via XRR compared to atomic force microscopy, where the probed area is usually only several hundred nanometres square.

EELS measurements were carried out on a dedicated VG 501 scanning transmission electron microscope (STEM) fitted with a spectrometer with a McMullan parallel EELS detection system [17]. The carbon K edge and the valence loss spectra were acquired for each sample at convergence semi-angle of 7.4 mrad and collection semi-angle of ∼7 mrad. This ensures that the sp^2 bonds are counted independently of their orientation [20]. The standard analysis [8,18,19] was then employed to obtain the single-scattering K-edge and plasmon peak, respectively. The π^* peak in the carbon K-edge was modelled with a gaussian, and its area was normalised to the experimental spectra. Referring this to the equivalent area for graphite, the sp^2 content is obtained [8,19,20], with 5% error. The plasmon energy results as a parameter from fitting the quasi-free electron model to the plasmon peak.

3. Result and discussion

3.1. X ray reflectivity

The refractive index for X-rays in solids is smaller than unity, so that total external reflection occurs at low angles of incidence. As the incidence angle θ_i increases above a critical angle θ_c, X-rays start to penetrate into the film. From Snell's law at the air/film interface, one can obtain the critical angle for a medium with two elements, carbon and hydrogen:

$$\theta_c=\lambda\sqrt{\frac{N_A r_0}{\pi}\rho\frac{[X_C(Z_C+f'_C)+X_H(Z_H+f'_H)]}{(X_C M_C+X_H M_H)}}, \quad (1)$$

where $r_0=e^2/4\pi\epsilon_0 m_e c^2$ is the classical electron radius, N_A is the Avogadro number, M_C and M_A are the carbon and hydrogen molar masses, f'_j takes dispersive corrections into account; ρ is the mass density and X_j is the atomic fraction. At $\lambda=1.3926$ Å, f'_C and $f'_H\sim 10^{-2}$. Thus, assuming $f'_j=0$, we obtain, with $X_H=1-X_C$:

$$\rho=\frac{\pi^2 c^2\epsilon_0}{3\lambda^2 N_A e^2}M_C m_e\theta_c^2\frac{11X_C+1}{5X_C+1}. \quad (2)$$

We note that the dependence on H content is quite small in the usual range $X_H=10–50\%$ (e.g. if $\theta_c=720''$ at $\lambda=$ 1.3926 Å, ρ is 2.3 g/cm^3 if $X_H=0.1$ and 2.16 g/cm^3 if $X_H=0.5$).

For a thin layer on a substrate (Fig. 1), the two rays reflected at the film surface and at the film–substrate interface can interfere, and from Snell's law, one can see that constructive interference is obtained when:

$$\theta_i^2=\theta_c^2+\frac{\lambda^2}{4d^2}(k+1/2)^2 \text{ when } n_1<n_2 \quad (3a)$$

or

$$\theta_i^2=\theta_c^2+\frac{\lambda^2}{4d^2}k^2 \text{ when } n_1>n_2, \quad (3b)$$

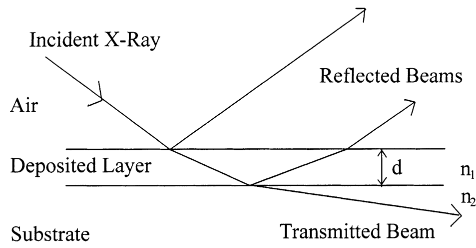

Fig. 1. Reflection of X-rays under grazing incidence from a single layer of refractive index, n_1, and thickness, d, on a substrate of refractive index, n_2.

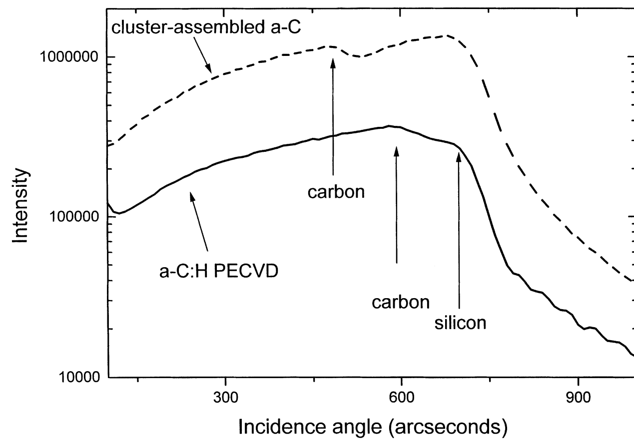

Fig. 2. Double critical angle in the cluster-assembled carbon film and in an a-C:H film.

Table 1
Density, thickness, and surface roughness of the ta-C+10 V film of Fig. 3b

	Density (g/cm^3)	Thickness (Å)	Roughness r.m.s.
Si			10
C	2.56	275	8
C	2.72	370	8
C	2.43	90	5

respectively, where d is the thickness and k is an integer. For $\theta_i > 2\theta_c$, the spacing between the fringes is $\Delta\theta \cong \lambda/2d$. Thickness can thus be found from the fringe period. This has been extended by Parrat to treat multiple interfaces and multilayers [14].

The ta-C:H films usually have a density (and therefore a critical angle) that is smaller than, or comparable to, the Si substrate density (2.33 g/cm^3), so that the Si critical angle is often seen, and not that of the film. The film only perturbs the shape of the critical angle. For films with a low density, a double critical angle is clearly distinguishable, thus allowing an easier determination of the density (Fig. 2).

Fig. 3 shows a typical XRR curve for ta-C:H. Only one fringe period is seen, showing that these films consist of a single layer. Very good simulations of the measured curves were obtained for the films (sometimes with a very small and less dense surface layer). The presence of a ≅1–2 nm layer of different density (possibly com-

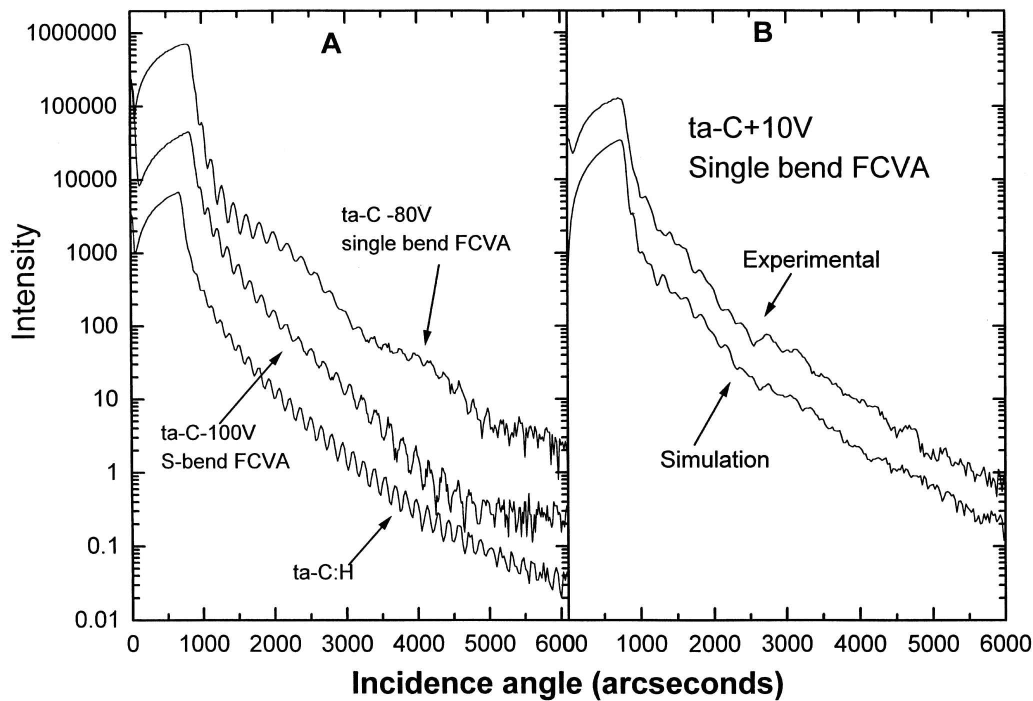

Fig. 3. (a) From top to bottom: reflectivity curve of the single bend FCVA ta-C −80 V; S-bend FCVA ta-C −100 V film; ta-C:H ECWR film. (b) Reflectivity curve of the ta-C +10 V film; the bottom line, shifted for clarity, is a simulation of the reflectivity curve. The resulting structure is detailed in Table 1.

Table 2
Film density, thickness, surface roughness and sp^3 content for the amorphous carbon films studied in this paper

Sample	Density (g/cm^3)	Thickness (Å)	Surface roughness r.m.s (±1 Å)	sp^3 content (±5%)
ta-C −290 V	2.86±0.02 (bulk)	Layered	7	76
ta-C −200 V	3.03±0.02 (bulk)	Layered	6	81
ta-C −80 V	3.24±0.02 (bulk)	635+70 (2.7 g/cm^3)	6.5	87
ta-C floating	2.91±0.02 (bulk)	Layered	8	78
ta-C +10 V	2.71±0.02 (bulk)	Layered (see Fig. 3b)	5	73
ta-c S-bend −300 V	3.17±0.03	700+20 (1.7 g/cm^3)	4	85
ta-c S-bend −100 V	3.26±0.03	760	8	88
ta-c S-bend −20 V	3.13±0.03	840	7	86
ta-C:H ECWR	2.13±0.03	955	5.5	70
a-C:H PECVD	1.63±0.035	≅2400	5	58
a-C 1 Mag. Sput.	1.72±0.035 (bulk)	Layered (see text)	5	–
a-C cluster-ass.	1–1.4	–	–	≈10

posed of Si, C, O [2,7]) at the film–substrate interface gives an even better fit. Ta-C:H films from the more capacitively coupled ECWR have a density in the range 2.3–2.4 g/cm^3, whilst the others have densities in the range 2.1–2.23 g/cm^3. A similar behaviour was obtained for a-C:H films, but with a clear double critical angle structure, giving a density of 1.64–1.74 g/cm^3.

For ta-C films, it is easier to determine the film density, as the critical angle is greater than the Si critical angle (Table 2). Densities of up to 3.26 g/cm^3 were obtained for an 88% sp^3 film from the S-bend FCVA. However, for the single-bend FCVA, the reflectivity curves show multiple periodicities, which indicate internal layering. They can be reproduced only by taking into account two or more layers with different densities. This is supported by cross-sectional high-resolution TEM measurements, which show similar layering for pulsed laser deposited ta-C [21]. In general, if a film consists of a bulk, dense layer and thinner and less dense layers at the top and the bottom, the critical angle is that of the bulk layer. Thus, from the critical angle, we directly obtain the density of the densest layer and not the average film density, which requires a fit of the multilayer structure.

The film grown at −80 V shows a smaller period corresponding to the overall film thickness and a larger period corresponding to a less dense surface layer ~7 nm thick [Fig. 3(a)]. Other films show more complex curves [Fig. 3(b)]. The number of layers, their density, thickness and roughness are all variable, and the density of the top and bottom layers (and maybe of the bulk) is probably not constant, whilst the sp^3 content does not vary so much with bias (Table 2). Simulation of such a structure is difficult. The optimum −80 V bias corresponds to the minimum thickness for the less dense layers.

However, ta-C films grown with the S-bend filter show a much higher uniformity and only a slight dependence of density and layering on the substrate bias (Table 2). Surface layers never exceed 1–2 nm. The thickest one, 2 nm, is seen for the film grown at a bias of −300 V.

The magnetron-sputtered a-C shows a clear double critical angle, corresponding to $\rho \cong 1.7(\pm 0.05)$ g/cm^3. The reflectivity curve exhibits three different periodicities, corresponding to ≅360 nm (total thickness), ≅40nm and ≅5 nm (surface layers) with ρ varying from 1.7 to 1.15 g/cm^3 in the surface layer. A clear double critical angle structure was detected for the nanostructured a-C, resulting in densities of ~1 to ~1.4 g/cm^3, depending on the size of the deposited clusters (Fig. 2) [13].

The top surface r.m.s. roughness was found to be in the range of 5–8 Å for all the films (Table 2), and no direct relationship between roughness and deposition parameters could be found.

3.2. EELS

The low energy loss spectrum is proportional to the energy loss function, which can be described, in the framework of the Jellium model and small scattering vector, as [18]:

$$\mathrm{Im}\left[\frac{-1}{\epsilon(E)}\right]=\frac{E(\Delta E_p)E_p^2}{(E^2-E_p^2)^2+(E\Delta E_p)^2}, \tag{4}$$

where $\epsilon(E)$ is the dielectric function, E_p is the plasmon energy and ΔE_p is the FWHM of the energy loss function. The plasmon energy is defined as:

$$E_p=\hbar\left(\frac{ne^2}{\epsilon_0 m^*}\right)^{1/2}. \tag{5}$$

To derive the mass density from the valence electron density, we assume that C contributes four valence electrons, and H contributes one electron, yielding:

$$\rho=\frac{M_C\epsilon_0}{12\hbar^2 N_A}m^* E_p^2\left(\frac{11X_C+1}{3X_C+1}\right). \tag{6}$$

The structure of Eqs. (2) and (6), giving the mass density via XRR and EELS, can be directly compared. In Eq. (2), the unknown parameters are the critical angle, θ_c, and carbon fraction, X_C, whilst m_e is the free electron mass. In Eq. (6), the unknowns are the plasmon energy, E_P, the carbon fraction X_C, and the electron effective mass, m^*. Eq. (2) has a weaker dependence on the H content ($5X_C$ instead of $3X_C$ at the denominator). The approximations used to obtain Eq. (6) are cruder than those for Eq. (2). The weaker point of Eq. (6) is the unknown electron effective mass that naturally arises from the assumption of a 'quasi-free' electron model. The usual approach is to derive m^* in Eq. (6) so that the density of diamond (3.515 g/cm^3) corresponds to its plasmon energy of 33.8 eV [8]. This gives $m^* \sim 0.8516 m_e$. However, some groups assumed $m^* = m_e$, thus considering the electrons totally free [9], introducing a ~15% difference in the calculated densities. Weiler et al. proposed a common sp^3-density relationship for ta-C and ta-C:H [22,23]. Closer inspection of the original data reveals that a different electron mass was used by Fallon et al. [8] and Weiler [22,23], $\sim 0.85 m_e$ and $1 m_e$, respectively, resulting in a ~15% overestimation of the density of ta-C:H. Our data from XRR on similar ta-C:H films indicate a maximum density of 2.39 g/cm^3 comparable with the ~2.4 g/cm^3 obtained on scaling by 15% the original data of Weiler.

XRR should be the method of choice to measure the mass density. It is superior not only to the plasmon energy approach, but also to other approaches such as floating measurements and RBS plus profilometry. Yet, EELS still remains the standard choice of measurement of the sp^3 fraction, at the same time yielding the plasmon energy. Using the independent mass determination from XRR, we can fit an effective electron mass that can be used to obtain a rough estimate of the density from the plasmon energy of all amorphous carbons. Thus, from Eq. (6), we plotted the reduced densities from XRR and EELS, $D = \rho_{XRR}(3X_C+1)/(11X_C+1)$ against $P = m_e M_C \epsilon_0 (12\hbar^2 N_A)^{-1} E_P^2$, to obtain a line with slope $m^*/m_e = 0.87$ (Fig. 4). This is the first direct evidence of the existence of a common effective mass for diamond and all amorphous carbons. Indeed, this gives E_p (diamond) ~33.4 eV, within the 0.5 eV experimental error. We can now give a relation between sp^3 and density, as shown in Fig. 5, where our data, together with those of Weiler and Fallon, are plotted, scaled with our fitted m^*.

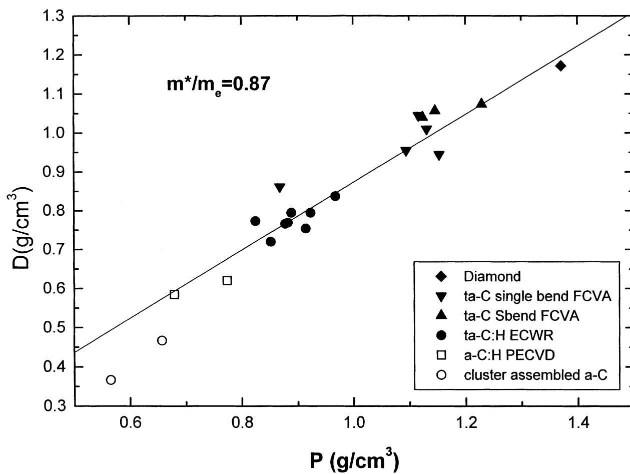

Fig. 4. Plot of $D = \rho_{XRR}(3X_C+1)/(11X_C+1)$ in function of $P = m_e M_C \epsilon_0 (12\hbar^2 N_A)^{-1} E_P^2$. The slope of the linear fit is m_e/m^*. The density of the cluster-assembled a-C with EELS is higher than that derived by XRR, due to their nanoporosity.

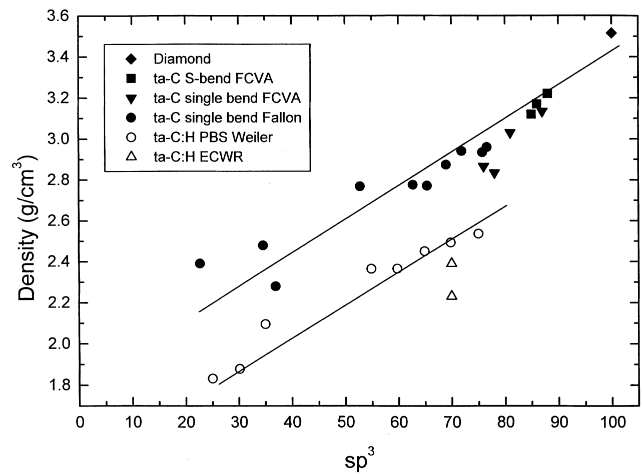

Fig. 5. Variation of sp^3 fraction and density for ta-C and ta-C:H films. The lines are a guide for the eye.

4. Conclusions

A wide variety of amorphous carbons have been analysed via XRR and EELS. XRR is shown to be the method of choice to measure their density and cross-sectional structure. Comparing XRR and EELS data for the first time, we have been able to fit a common effective mass for all amorphous carbons and diamond, validating the jellium approach to density from plasmon energy. We have thus shown the correct general relationship between sp^3 and mass density for ta-C and ta-C:H.

The cross-sectional structure of hydrogenated films is found to be quite uniform, with less than 1–2 nm interface and eventually surface layers. Ta-C can possess a heavily layered structure, depending on the deposition conditions. Our S-bend FCVA is found to give the most uniform ta-C films. Plasmon energy is convenient to yield the average density of heavily layered films when fitting of XRR data is difficult.

Acknowledgements

The authors thank B. Kleinsorge, M.C. Polo, S.E. Rodil, N.A. Morrison, N. Conway, J. Seekamp, X.L.

Peng, P. Milani for carbon samples and E. Riedo for plasmon energy of cluster assembled a-C. A.C.F. acknowledges funding from an EU Marie Curie fellowship.

References

[1] F. Toney, S. Brennan, J. Appl. Phys. 66 (1989) 1861.
[2] A. Lucas, T.D. Nguyen, J.B. Kortright, Appl. Phys. Lett. 59 (1991) 2100.
[3] S. Logothetidis, G. Stergioudis, Appl. Phys. Lett. 71 (1997) 2463.
[4] Q. Zhang, S.F. Yoon, J. Ahn, H. Yang, D. Bahr, J. Appl. Phys. 86 (1999) 289.
[5] B. Lengeler, in: M. Campagna, K. Rosei (Eds.), X-ray Absorption and Reflection in the Hard X-Ray Range, North Holland, Amsterdam, 1990.
[6] C.A. Davis, K.M. Knowles, G.A.J. Amaratunga, Phys. Rev. Lett. 80 (1998) 3280.
[7] D.R. McKenzie, D. Muller, B.A. Pailthorpe, Phys. Rev. Lett. 67 (1991) 773.
[8] P.J. Fallon, V.S. Veerasamy, C.A. Davis, J. Robertson, G.A.J. Amaratunga, W.I. Milne, J. Koskinen, Phys. Rev. B 48 (1993) 4777.
[9] R. Lossy, D.L. Pappas, R.A. Roy, J.P. Doyle, J.J. Cuomo, J. Bruley, J. Appl. Phys. 77 (1995) 4750.
[10] M.C. Polo, J.L. Andujar, A. Hart, J. Robertson, W.I. Milne, Diamond Relat. Mater. 9 (2000) 663.
[11] N.A. Morrison, S.E. Rodil, A.C. Ferrari, J. Robertson, W.I. Milne, Thin Solid Films 337 (1999) 71.
[12] N.M.J. Conway, A. Ilie, J. Robertson, W.I. Milne, A. Tagliaferro, Appl. Phys. Lett. 73 (1998) 2456.
[13] P. Milani, M. Ferretti, P. Piseri, C.E. Bottani, A.C. Ferrari, A. Li Bassi, G. Guizzetti, M. Patrini, J. Appl. Phys. 82 (1997) 5793.
[14] L.G. Parrat, Phys. Rev. 95 (1954) 359.
[15] M. Wormington, I. Pape, T.P.A. Hase, B.K. Tanner, D.K. Bowen, Phil. Mag. Lett. 74 (1996) 211.
[16] S.K. Sinha, E.N. Sirota, S. Garoff, Phys. Rev. B 38 (1988) 2297.
[17] D. McMullan, P.J. Fallon, J. Ito, A.J. McGibbon, in: Electron Microscopy, EUREM 92, Granada, Spain Vol. 1 (1992) 103.
[18] R.F. Egerton, Electron Energy Loss Spectroscopy in the Electron Microscope, Plenum, New York, 1996.
[19] S.D. Berger, D.R. McKenzie, P.J. Martin, Phil. Mag. Lett. 57 (1988) 285.
[20] N.K. Menon, J. Yuan, Ultramicroscopy 74 (1998) 83.
[21] M.P. Siegal, J.C. Barbour, P.N. Provencio, D.R. Tallant, T.A. Friedmann, Appl. Phys. Lett. 73 (1998) 759.
[22] M. Weiler, S. Sattel, T. Giessen, K. Jung, H. Ehrhardt, V.S. Veerasamy, J. Robertson, Phys. Rev. B 53 (1996) 1594.
[23] M. Weiler, Ph.D. thesis, Universität Kaiserslautern, 1994.